Kim et al. *NPG Asia Materials* (2024)16:7
https://doi.org/10.1038/s41427-023-00527-3

NPG Asia Materials

ARTICLE Open Access

An advanced 3D lymphatic system for assaying human cutaneous lymphangiogenesis in a microfluidic platform

Minseop Kim[1], Sieun Choi[1], Dong-Hee Choi[2], Jinchul Ahn[2], Dain Lee[1], Euijeong Song[3], Hyun Soo Kim[4], Mijin Kim[5], Sowoong Choi[5], Soojung Oh[4], Minsuh Kim[2,3], Seok Chung[1,2,6] and Phil June Park[4]

Abstract

The human cutaneous lymphatic system strictly controls lymphatic functions by coordinating with skin cells. The lymphatic system plays important roles in removing cell waste, residual proteins, various antigens, and immune cells from tissues to maintain homeostasis and activate the immune system through the drainage of interstitial fluid[1,2]. The skin protects our body from external stimuli such as pathogens through the cutaneous lymphatic system[3,4]. Herein, to develop an in vitro human cutaneous lymphatic model, we present two 3D microfluidic platforms: a lymphangiogenesis model with a precollecting lymphatic vessel-like structure and an advanced lymphangiogenesis model with a functional cutaneous barrier and a precollecting lymphatic vessel-like structure. In addition, we rapidly analyzed prolymphangiogenic effects using methods that incorporate a high-speed image processing system and a deep learning-based vascular network analysis algorithm by 12 indices. Using these platforms, we evaluated the pro-lymphangiogenic effect of Lymphanax, a natural product derived from fresh ginseng. As a result, we demonstrated that Lymphanax induces robust lymphangiogenesis without any structural abnormalities. In conclusion, we suggest that these innovative platforms are useful for studying the interaction between the skin and lymphatic system as well as evaluating the prolymphangiogenic effects of drugs and cosmetics.

Introduction

The lymphatic system is a 'drainage system' that removes interstitial fluid containing wastes, antigens, and immune cells from tissue in the body[1,2]. Our body maintains the homeostasis of this drainage activity by controlling the proliferation of lymphatic endothelium with tube formation, called lymphangiogenesis[5]. Lymphatic endothelial cells (LECs) express the receptor tyrosine kinase vascular endothelial growth factor receptor 3 (VEGFR3), which binds vascular endothelial growth factor C (VEGF-C). The stimulation of the VEGF-C gradient activates the proliferation and migration of LECs, which induces neolymphatic vessels to sprout from pre-existing lymphatic vessels[6,7]. The lymphatic vessel structure formed by LECs allows the drainage of interstitial fluid, resulting in the regulation of peripheral tolerance and protective immunity[8,9]. Lymphangiogenesis occurs dynamically under abnormal conditions, such as inflammation, wound healing, and tumors[10,11]. In particular, the skin coordinates rapid responses to external challenges through immune surveillance in the lymphatic system. Because skin produces large amounts of interstitial fluid in a day, the cutaneous lymphatic vessels are densely located under the epidermis to promptly eliminate the interstitial fluid[12,13]. The failure to drain interstitial fluid in skin causes several problems, such as loss of elasticity or development of inflammation[14].

Correspondence: Minsuh Kim (dong1118@korea.ac.kr) or Seok Chung (sidchung@korea.ac.kr) or Phil June Park (mosme@amorepacific.com)
[1]KU-KIST Graduate School of Converging Science and Technology, Korea University, Seoul 02841, Republic of Korea
[2]School of Mechanical Engineering, Korea University, Seoul 02841, Republic of Korea
Full list of author information is available at the end of the article
These authors contributed equally: Minseop Kim, Sieun Choi

The cellular dynamics and molecular mechanisms of three-dimensional (3D) neolymphatic vessel formation are difficult to represent in the present conventional in vitro 2D cell culture models with extracellular matrix (ECM)-coated dishes[15]. In vivo models more reflect complexities more effectively than conventional in vitro models in 3D, but these models require considerable time and money and have difficulties in the interpretation of human physiological results[15,16]. Microfluidic chips might be an intriguing research model that can offer numerous applications in the biology research field by providing a diverse culture environment subdivided into several channels containing ECM and/or cells[17,18]. Microfluidic chip culturing LECs in 3D ECM allowed us to investigate and regulate lymphangiogenesis[19,20]. In this paper, we explored a microfluidic model culturing LEC monolayers to verify the effect of a new natural substance termed Lymphanax, a thermally converted *Panax ginseng* root extract, on prolymphangiogenesis.

Recently, it has been reported that ginseng improves lymphangiogenesis and lymphatic circulation. Total saponins of panaxnotoginseng (PNS), a mixture isolated from PNS, increase VEGF-C expression in LECs and activate lymphangiogenesis[21]. Additionally, it has been shown that ginsenoside Rg1, a component of saponin in ginseng, promotes prolymphangiogenic activity through the VEGF-C/VEGFR-3 mechanism, resulting in enhanced lymphatic transport[22]. Lymphanax can, therefore, be a new candidate to maintain the condition of the lymphatic system. In this paper, we showed that Lymphanax had a prolymphangiogenic effect on 3D lymphatic vessels. Morphological changes in their complicated 3D structure could be automatically quantified with a deep learning-based algorithm. The lymphatic vessels were aligned with the functional cutaneous barrier by coculturing LECs and keratinocytes in the microfluidic chip. The microfluidic model formed a thick skin layer and lymphatic vessels together and showed the prolymphangiogenic effect of Lymphanax with the cutaneous barrier. As a result, Lymphanax induced lymphangiogenesis through keratinocytes without abnormal lymphatic conditions. Lymphanax was found to promote physiological changes in lymphatic vessels beneath the skin. These results demonstrated that our microfluidic model can be used for evaluating the potential pharmacological ability of a new substrate in the cutaneous lymphatic system.

Materials and methods

Fabrication of the microfluidic chip

The microfluidic devices were fabricated by soft lithography. The SU-8-100 photoresist spin-coated 16-inch silicon wafer was baked at 95 °C for 1 h, and then, microfluidic channels were patterned by selectively exposing ultraviolet (UV) light through a mask. A polydimethylsiloxane (PDMS; Dow Chemical, Sylgard 184) solution, which is a representative biocompatible substance[23], was poured on the wafer and cured at 80 °C for over 1 hour in a dry oven. The wafer was coated with polytetrafluoroethylene, and the PDMS curing could be repeated more than 80 times. After the cured PDMS was detached from the wafer, reservoirs were punched using 3 mm and 1 mm biopsy punches. The punched PDMS and cover glass were sterilized at 120 °C for 30 minutes and then dried at 80 °C overnight. The dried cover glass was bonded onto the PDMS with an oxygen plasma treatment (FEMTO Science). Then, the hydrophilic microchannels were coated with 2 mg/mL biocompatible PDA solution[24] and incubated at 37 °C for 1 hour 30 minutes. After the channels were washed with deionized distilled water (DDW) twice, the microfluidic chip was dried at 80 °C overnight to allow the microchannels to be hydrophobic. Collagen type 1 (COL1) solution (Corning, 354236) at 2 mg/ml, 3 mg/ml, and 5 mg/ml was prepared by mixing with 10X phosphate buffered saline (PBS) and DDW. In addition, sodium hydroxide (NaOH, 1 N) was added to adjust the pH to 7.4. The mixed COL1 solutions were injected inside of each of the 3 ECM gel channels in series and incubated at 37 °C for 40 minutes for gelation. After that, the medium channels were filled with cell culture medium.

Cell preparation

For lymphatic endothelial cell experiments, human dermal lymphatic endothelial cells and juvenile foreskin (HDLEC; Promocell, C-12216) were purchased and cultured in an EGM2-MV bullet kit (Lonza, CC3202) at 37 °C in a humidified 5% CO_2 incubator. For keratinocyte experiments, Human Epidermal Keratinocyte, Adult, Single Donor (NHEK-Ad; Lonza, 00192627) were purchased and cultured with the KGM Gold Keratinocyte Growth Medium BulletKit (Lonza, 00192060). HDLECs and NHEKs were grown to ~ 70% and ~ 80% confluence in 75 T flasks, respectively.

Cell culture in a microfluidic chip

For lymphatic endothelial barrier formation, HDLECs were detached using Accutase (Innovative Cell Technologies, AT104) at 37 °C for 10 minutes, and the cell suspension was prepared at a density of 2×10^6 cells/ml. All medium in the microfluidic chip was removed, and 40 µl of the cell suspension was injected into each lymphatic seeding channel. Then, the devices were tilted by 30° at 37 °C for 1 hour so that HDLECs could be attached mainly to the COL1 hydrogel wall. Subsequently, unattached HDLECs were eliminated, and then, all medium channels were filled with fresh medium. After the lymphatic single layer was established for 2 days, lymphangiogenesis was induced for the next 6 days.

Since KGM Gold medium contains 5% more fetal bovine serum (FBS) than EGM-2 MV medium, KGM Gold with 5% FBS was used from this stage. This medium was supplemented with 100 nM sphingosine-1-phosphate (S1P; Sigma, 73914) for all four conditions, 100 ng/ml of vascular endothelial growth factor-A (VEGF-165; PeproTech, 100-20) and VEGF-C (PeproTech, 100-20CD) except for the negative control. For combined treatment, 50 ng/ml and 250 ng/ml Lymphanax were added to the medium of the V100 + L50 and V100 + L250 conditions, respectively. In addition, considering that Lymphanax was dissolved in 10% DMSO solution, the DMSO ratio of all culture media was adjusted to be the same.

For the skin and lymphatic endothelial barrier coculture system, NHEKs were detached using Accutase at 37 °C for 10 minutes, and the cell suspension was prepared at a density of 2.4 × 10^6 cells/ml. All medium in the microfluidic chip was removed, and 40 μl of the cell suspension was injected into each skin seeding channel. NHEKs were cultured for 3 days to form a skin barrier, and HDLECs were introduced to the lymphatic seeding channel. After we confirmed that the HDLECs were well attached, an air-liquid interface was established by removing KGM Gold from the skin seeding channel and tilting the device above 45°. Moreover, ascorbic acid (Sigma, AA4403), which can enhance the differentiation of keratinocytes, was added. Induction of lymphangiogenesis began on D5, which was 2 days after HDLECs were seeded.

Immunofluorescence staining

Cells in the devices were fixed with 4% paraformaldehyde (PFA; Biosesang, PC2031-100-00) for 30 minutes and permeabilized with 0.2% Triton X-100 (Sigma, T8787) for 5 minutes at room temperature. Then, the cells were blocked using 5% bovine serum albumin (BSA, Sigma, A9418) for 90 minutes at room temperature. Forty microliters of primary antibody solution diluted in PBS containing anti-LYVE1 (1:100, Thermo Fisher Scientific, MA5-32512), anti-RELN (1:100, Thermo Fisher Scientific, PA5-78413), anti-PROX1 (1:100, Invitrogen, PA5-85552), anti-VE cadherin (1:100, Abcam, ab33168), anti-VEGFR3 (1:100, Thermo Fisher Scientific, MA5-15651), anti-CD31 (1:200, Abcam, ab24590), anti-Ki67 (1:500, Abcam, ab15580), anti-K10 (1:100, Abcam, ab76318), anti-K14 (1:100, Abcam, ab7800), and anti-Loricrin (1:200, Novus Biologicals, NBP1-33610) in PBS was added to each channel and stored at 4 °C overnight. After that, appropriate secondary antibodies at 1:200 dilutions were added to the samples for 2 hours at room temperature. For staining of F-actin and DNA, 1:500 diluted phalloidin and DAPI in PBS were added. All procedures were performed with devices rocking gently on a shaker, and three sets of PBS washes were included in each step. Images were obtained using a confocal microscope (Carl Zeiss, LSM-700).

Quantification of lymphangiogenesis

All images used for analysis were immunostained with phalloidin and captured using Celena® X (Logos Biosystems). Due to their tree-like form, vascular networks can be structurally categorized as branches and nodes. Since the innermost layer of a vessel consists of endothelial cells that combine to form a tube, branches and nodes consist of multiple endothelial cells and have a 3D structure[25–27]. Based on F-actin-stained images (1600 × 1200 pixels), 3D lymphangiogenic morphogenesis was quantified by 12 indicators. The algorithm recognized the sprouting region between nodes as a branch. Curvature refers to the curvature of a branch; Bra. Area refers to the area of a branch; Nod.Rad refers to the radius of a node; Bra.Euc.Leng refers to the Euclidian distance between the endpoints of each branch; Bra.-Width refers to the average width of a branch; N.C.B. refers to the number of branches connected to a node; Bra.Length refers to the total distance between the endpoints of each branch; Bra.Num indicates the number of branches; Area refers to the area of the entire vasculature; Nod.Num refers to the number of nodes; Bra.Δ.Width refers to the mean value of width differentiation at each branch point. For manual image analysis, values of whole vessels containing several branches were measured using ImageJ software. Ves.Num refers to the number of vessels; Area refers to the area of the entire vessel; Ves.Leng indicates the total distance from the starting point to the endpoint of each vessel in a straight line; Separation refers to the number of vessels separated from the vessel divided by the total Ves.Num. The code for this algorithm was released on GitHub[28]. [https://github.com/moonchildz/angio_analysis].

Preparation of lymphanax

For Lymphanax, fresh ginseng was washed 3 times and dried for 30 minutes. The ginseng was then cut to 1 cm long, cultured in anaerobic conditions for 3 weeks, and dried under hot air at 60 °C. Subsequently, Lymphanax was immersed in 50%-80% EtOH at 50–80 °C for 5 hours. After this process was repeated 3 times, the extracted material was vacuum filtered, concentrated and purified with a rotary evaporator. The obtained Lymphanax was dissolved in DMSO and ready for cell treatment.

Permeability analysis

For measurement of the permeability of the skin layer in the microfluidic chip, 10 μM 0.4 kDa fluorescein sodium salt (Sigma, F6377), 4 kDa fluorescein isothiocyanate-dextran (FITC-dextran; Sigma, FD4), and 40 kDa fluorescein isothiocyanate-dextran (FITC-dextran; Sigma, FD40S) solutions were added to the medium channel of the skin layer. Fluorescence images of the gel channel

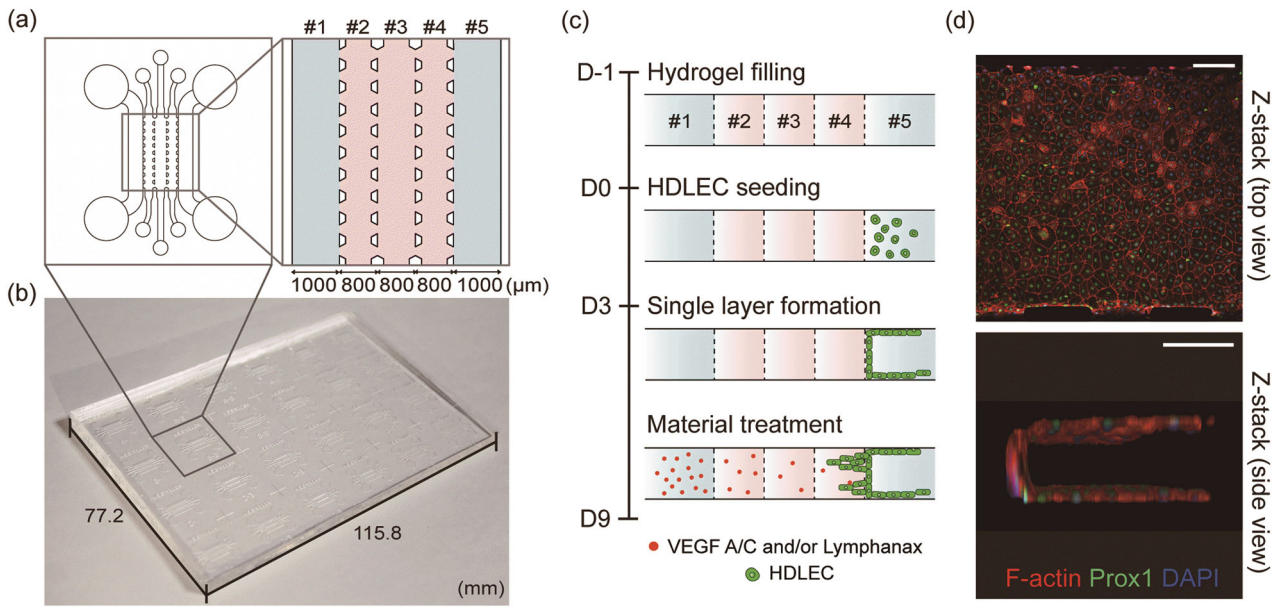

Fig. 1 A high-throughput microfluidic device for reproducing three-dimensional lymphangiogenesis in vitro. a Schematic design of each chip of the high-throughput device. The channels painted blue are media channels, and pink channels are gel channels. Media channels were filled with media containing cytokines and cells. Gel channels were filled with each concentration of collagen type I. **b** Top view of the whole 24-well PDMS high-throughput microfluidic device. This device included 24 lymphangiogenesis chips. **c** Experimental flow diagram of lymphangiogenesis modeling. Each gel channel was filled with seeding cells. The HDLECs were seeded in channel #5 and cultured for three days. After the formation of the HDLEC single layer, the cells were treated with Lymphanax for six days. **d** Immunofluorescence images of the HDLEC single layer on Day 3. The image above is a top view of the HDLEC single layer, and the image below is a side view of the HDLEC single layer. Prox1 (green) is expressed in lymphatic cells and HDLECs. The localization of HDLEC was indicated by F-actin (Red). Scale bars indicate 200 μm.

immediately next to the skin layer were captured after 0 min, 60 min, and 120 min of incubation at 37 °C. The intensity profile of diffusion was measured by ImageJ software, and then, the permeability value P was calculated using Fick's first law as follows:

$$J = -D\frac{\partial C}{\partial x}$$

$$Flux = -P\Delta C$$

where J is the flux, D is the diffusion coefficient, C is the concentration, x is the position, and P is the permeability of the skin layer.

Statistical analysis

Data are presented as the mean ± standard error of the mean (SEM), and statistical significance was determined using GraphPad Prism software (version 5.01). Comparisons among the groups were determined by one-way analysis of variance (ANOVA) followed by post hoc pairwise comparison testing using Tukey's method. Significance was defined as follows: $^{*}p < 0.05$, $^{**}p < 0.01$, and $^{***}p < 0.001$.

Results

A microfluidic device for inducing human dermal lymphangiogenesis was used to evaluate the prolymphangiogenic effect of lymphanax

The cutaneous lymphatic system is located in the hypodermis, the deepest of the three major skin layers of epidermis, dermis and hypodermis. We designed a microfluidic chip with five channels defined by posts to maintain the air-liquid meniscus and confine the filled liquid to the desired channel (Fig. 1a, S1a). Twenty-four chips were arrayed in 77.2 mm * 115.8 mm format to increase the experiment throughput (Fig. 1b, S1b). In the lymphangiogenesis application, type I collagen hydrogel (COL1) was filled in channel #4 and gelled, and human dermal lymphatic endothelial cells (HDLECs) were seeded in channel #5 (Fig. 1c), allowing attachment to the COL1 wall (Fig. 1c). Other channels were filled with medium containing growth factors and/or Lymphanax to create a gradient toward the HDLEC monolayer. The preparation processes for the chip are described in the Methods section and the supplementary information (Fig. S1c). After three days of culture, a confluent HDLEC monolayer was formed (Fig. 1c, d, S1d). The channel was designed to have a height of 150 μm to form an HDLEC vessel with a diameter comparable to that of the precollecting

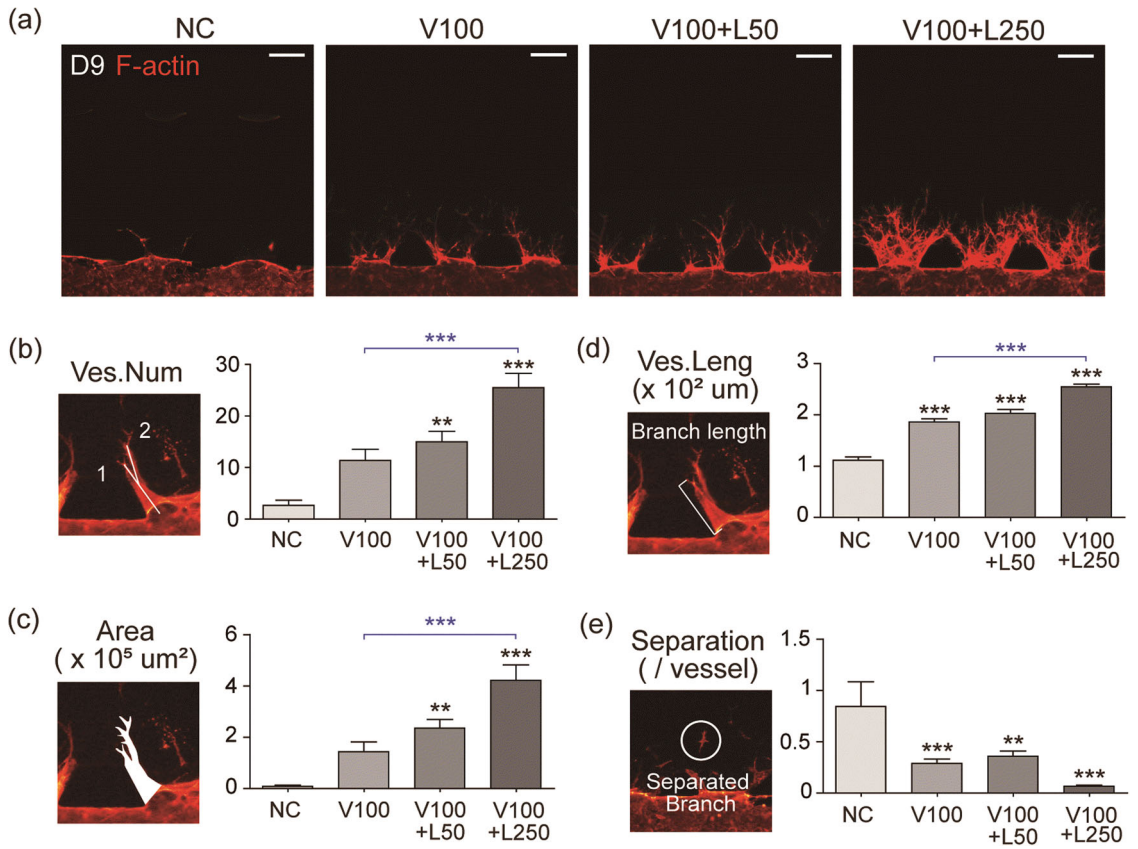

Fig. 2 Prolymphangiogenic effect assay on the high-throughput lymphangiogenesis model. a Immunofluorescence images showing lymphangiogenesis induced under each condition on Day 9. The area under the posts is channel #5, which was covered by an HDLEC single layer. Neolymphatic vessels sprout toward the 2 mg/ml collagen channel. The localization of HDLECs is indicated by F-actin (red). Scale bar indicates 200 μm. **b**–**e** The value of manual quantification for lymphangiogenesis under each condition. The average number of vessels (Ves. Num) in images (**b**). The average area of total vessels in images (**c**). The average length of vessels (Ves. Leng) in images (**d**). The number of separated tip cells that are not connected to the stalk cells in images (**e**). ($n = 6$ for the NC condition, $n = 8$ for the conditions). For comparison with each group and the NC (*, black) or Lymphanax-treated group and V100 group (*, blue), the p-value was determined by one-way ANOVA. *$p < 0.05$, **$p < 0.01$, and ***$p < 0.001$.

lymphatic vessel in vivo[1]. VEGF-A/C (100 ng/ml) in other channels (channel #1 in Fig. 1c) stimulated lymphangiogenesis, and the VEGF-A/C gradient induced the growth of lymphatic capillaries toward the gradient (Fig. 2a, S2a).

A strong lymphangiogenic response to VEGF-A/C and a 250 μg/ml Lymphanax (V100 + L250) gradient was indicative of the lymphangiogenic effects of Lymphanax compared to VEGF-A/C alone (V100) and VEGF-A/C with 50 μg/ml of Lymphanax (V100 + L50) (Fig. 2a, S2a). The pro-lymphangiogenic effect of Lymphanax was quantified using images acquired with a high-speed image processing system. Four indices, vessel number, total vessel area, vessel length and separated tip cell number per vessel, were manually measured (Fig. 2b–e). Notably, the number of neolymphatic vessels and the area of neolymphatic vessels increased significantly in the V100 + L250 group compared to the negative control (NC) and V100 groups (Fig. 2b-d). Additionally, the number of separated tip cells from vessels per branch was reduced in the V100 + 250 group. A steep gradient of VEGF-A/C activates tip cells and induces vigorous migration away from main vessels[29], but with Lymphanax, this treatment appears to induce lymphangiogenesis while simultaneously enhancing the structural stability of lymph vessels (Fig. 2e). The lymphangiogenic response to VEGF-A/C and 250 μg/ml Lymphanax was stronger than the lymphangiogenic response to VEGF-A/C and 50 μg/ml Lymphanax (Figs. 2, 3, 7). On the basis of the observed comparative effectiveness, it can be inferred that a dose of 100 μg/ml will be less effective than a dose of 250 μg/ml.

Lymphanax induced morphological and physiological changes in 3D lymphatic vessels

Using a deep learning-based algorithm, we quantified the physiological 3D changes in lymphangiogenic structures (Fig. 3)[27]. Treatment with 250 μg/ml Lymphanax

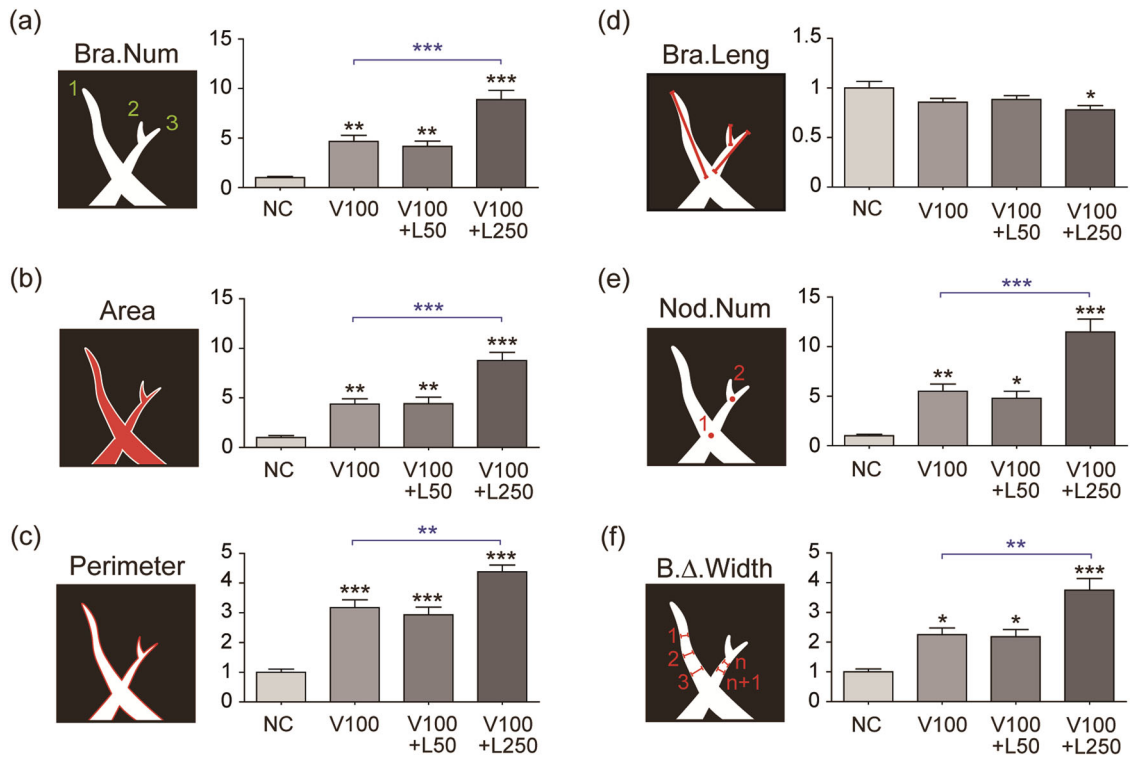

Fig. 3 The pro-lymphangiogenic effect of Lymphanax was verified by automatic morphological analysis of branches of neolymphatic vessels using a vascular vessel network analysis algorithm. a Branch number (Bra. Num) means the average number of total branches in images. **b** Area means average area of total branches in images. **c** Perimeter indicates the average value of the perimeter of vessels in the images. **d** Branch length (Bra. Leng) indicates the average length of the total branches in the images. **e** Node number (Nod. Num) means the average number of nodes formed by connected branches in images. **f** Branch width differentiation (B. Δ. Width) means the average branch width differentiation in images. ($n = 18$ for the NC condition, $n = 20$ for the other conditions). For comparison with each group and the NC (*, black) or Lymphanax-treated group and V100 group (*, blue), the *p-value* was determined by one-way ANOVA. *$p < 0.05$, **$p < 0.01$, and ***$p < 0.001$.

increased the number of branches and their perimeter and area, as shown by 12 indices (Fig. 3a–c). Intriguingly, branch length or the distance between two neighboring nodes did not change, indicating that Lymphanax treatment primarily stimulated lymphangiogenesis by increasing the number of nodes and not by branch length between neighboring nodes (Fig. 3d). Under VEGF-A/C, Lymphanax, and mixed gradients, the structural similarity between lymph node branches was maintained. In conclusion, treatment of 250 μg/ml Lymphanax with VEGF-A/C increases the sprouting of new lymphatic vessels (Fig. 3e) and the number of neolymphatic vessels by increasing their complexity and adding new nodes. The application of Lymphanax also increased the mean value of width differentiation at each branch point (Fig. 3f).

Indices describing the 3D lymphatic structure of lymphatic vessels revealed that Lymphanax did not induce significant morphological deformation (Fig. 4a–e). This finding indirectly demonstrated that the VEGF and Lymphanax gradient induced the formation of neolymphatic vessels without affecting their fundamental normal structure. Intriguingly, the number of branches attached to a node increased marginally in the V100 + L250 group (Fig. 4f). Immunofluorescence (IF) images confirmed the expression of lymphatic endothelial cell markers, including LYVE1 (lymphatic vessel endothelial hyaluronan receptor 1)[30], PROX1 (prospero homeobox protein 1)[31] and VEGFR3[32], as well as a pan-endothelial marker, CD31[33], in both the V100 and V100 + L250 groups (Fig. 5). Reelin (RELN), an extracellular matrix protein secreted by lymphatic endothelial cells[34], VE-cadherin (vascular endothelial cadherin)[35], and the proliferation marker Ki67[36] were also maintained in both groups (Fig. 5, S2b, c). Despite their activated lymphangiogenesis, the additional Lymphanax gradient-induced lymphatic vessels maintained normal lymphatic characteristics. Under Lymphanax treatment, the expression of button-like lymphatic endothelial cell junctions was also observed (Fig. S2c).

Reconstitution of the cutaneous lymphatic system

The cutaneous barrier is a physical barrier that protects the body from external damage[3,4]. To confirm that Lymphanax can affect the lymphatic system beneath the cutaneous

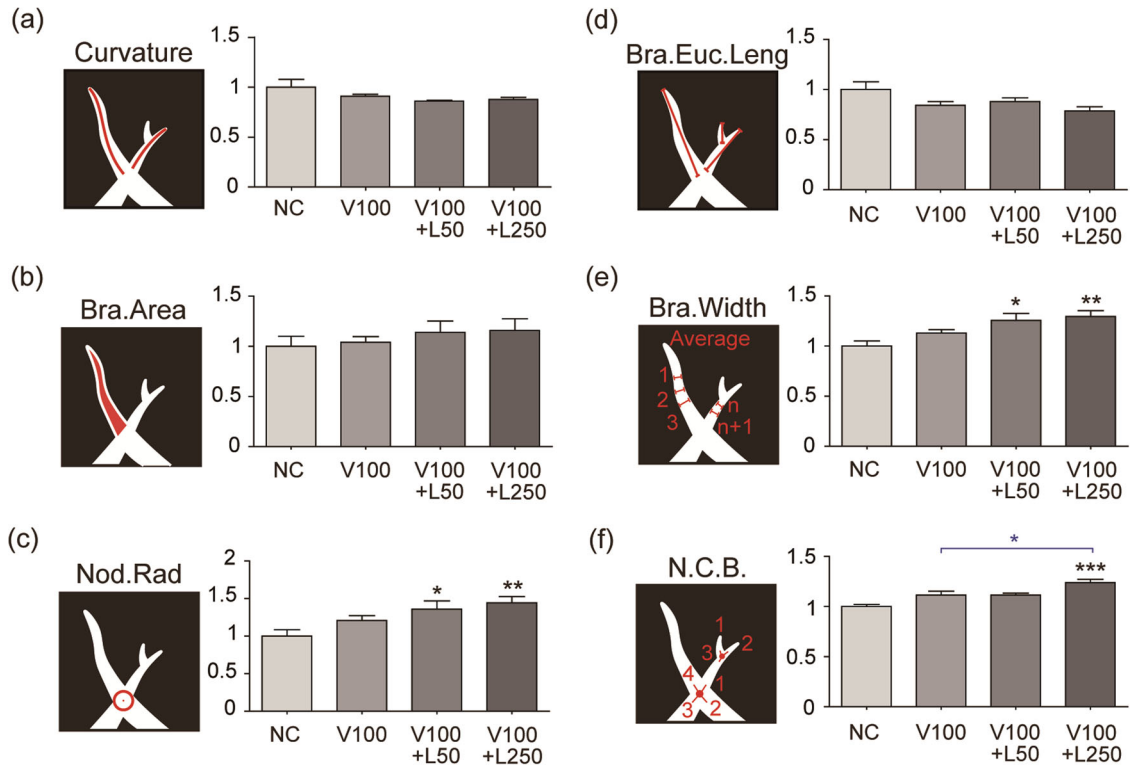

Fig. 4 Structural abnormality examination for neolymphatic vessels induced by Lymphanax using the vascular vessel network analysis algorithm. a Curvature means the average degree of curvature of branches in images. **b** Branch area (Bra. Area) means the average area of a single branch in the images. **c** Node radius (Nod. Rad) indicates the average size of the node radius in the images. **d** Branch Euclidean length (Bra. Euc. Leng) means the average straight length of branches in images. **e** Branch width (Bra. Width) means the average width of branches in images. **f** Node connected branch (N.C. B) is the average number of nodes connecting branches in the images. ($n = 18$ for the NC condition, $n = 20$ for the other conditions). For comparison with each group and the NC (*, black) or Lymphanax-treated group and V100 group (*, blue), the p-value was determined by one-way ANOVA. *$p < 0.05$, **$p < 0.01$, and ***$p < 0.001$.

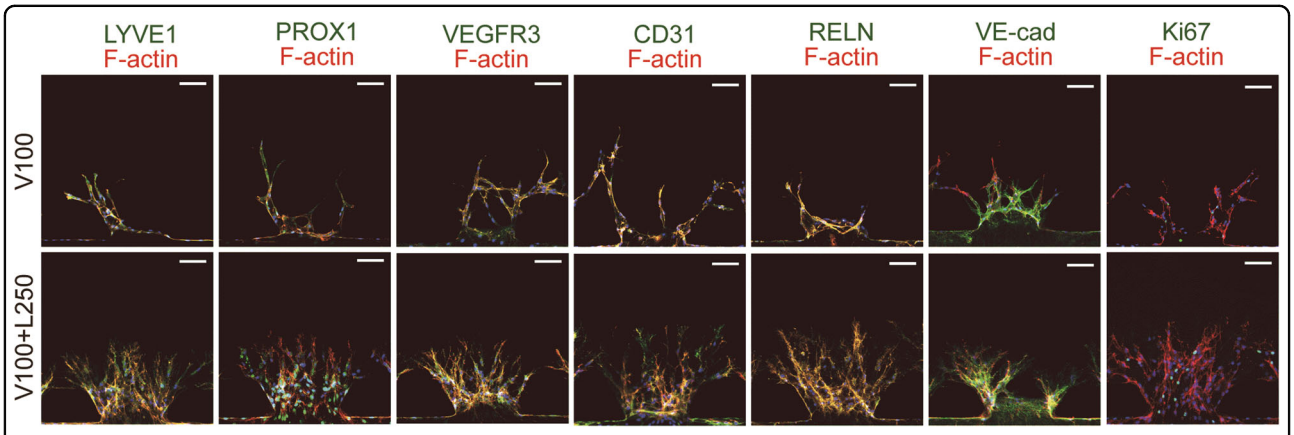

Fig. 5 Neolymphatic vessels induced by Lymphanax maintained the original characteristics of lymphatic vessels. Neolymphatic vessels induced by Lymphanax expressed protein markers indicating characteristics of lymphatic vessels: lymphatic vessel endothelial hyaluronan receptor 1 (LYVE1), Prospero homeobox protein 1 (PROX1), vascular endothelial growth factor receptor 3 (VEGFR3), CD31, reelin (RELN), vascular endothelial cadherin (VE-cad), and Ki67. F-actin (red) indicates the location of each cell. Immunofluorescence images of neolymphatic vessels were obtained under V100 and V100 + L250 conditions. Scale bars indicate 100 μm.

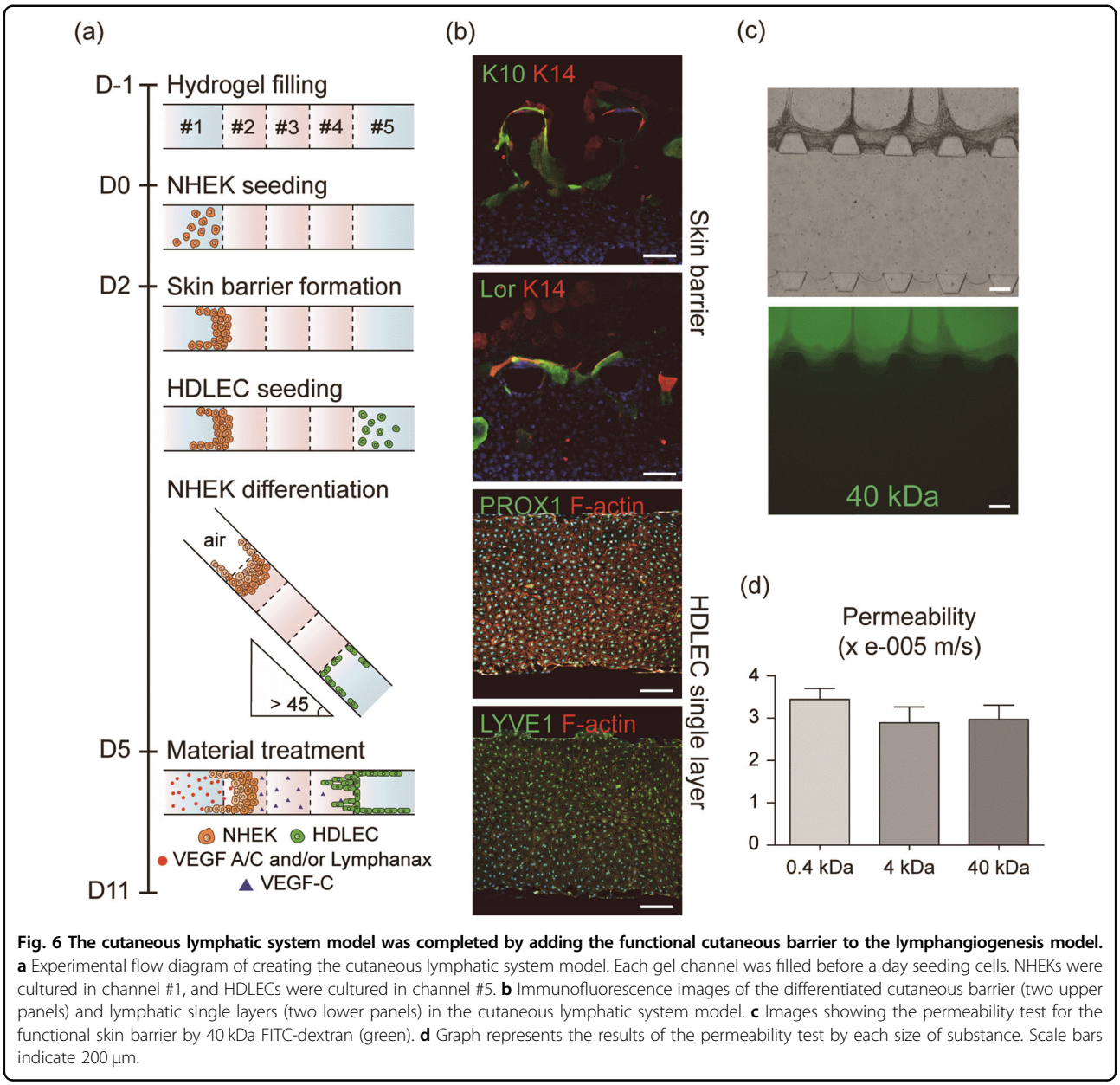

Fig. 6 The cutaneous lymphatic system model was completed by adding the functional cutaneous barrier to the lymphangiogenesis model. **a** Experimental flow diagram of creating the cutaneous lymphatic system model. Each gel channel was filled before a day seeding cells. NHEKs were cultured in channel #1, and HDLECs were cultured in channel #5. **b** Immunofluorescence images of the differentiated cutaneous barrier (two upper panels) and lymphatic single layers (two lower panels) in the cutaneous lymphatic system model. **c** Images showing the permeability test for the functional skin barrier by 40 kDa FITC-dextran (green). **d** Graph represents the results of the permeability test by each size of substance. Scale bars indicate 200 μm.

barrier, we added normal human epidermal keratinocytes (NHEKs) in channel #1 and lymphatic vessels in channel #5 (Fig. 6a). Gel channels between the NHEKs and lymphatic vessels were individually filled with 3 mg/ml, 5 mg/ml and 2 mg/ml type I collagen (COL1). The concentration of COL1 in two gel channels adjacent to the cutaneous layer (3 mg/ml and 5 mg/ml) was optimized for the formation of a stable cutaneous layer, while the concentration in the gel channel adjacent to the lymphatic vessel was optimized for the formation of a confluent lymphatic monolayer. NHEKs grew on 3 mg/ml COL1 (Fig. 6a, S3a). As they expanded, NHEKs formed a cutaneous barrier, invaded 3 mg/ml COL1 and reached 5 mg/ml COL1 (Fig. 6a, b). COL1 (3 mg/ml) induced stable collapse of the cutaneous monolayer, whereas COL1 (5 mg/ml) minimized the additional collapse of the hydrogel, preventing the NHEKs from coming into direct contact and disrupting the lymphatic vessels until Day 12, which is beyond the total experimental period (Fig. S3a, b). The 2 mg/ml COL1 concentration was chosen for HDLECs that formed confluent monolayers and sprouted lymphatic vessels. Interestingly, NHEKs did not form a thick cutaneous barrier without 3 mg/ml COL1 (Fig. S3c, d). The optimal combination of three COL1s allowed the reproduction of the structure of human skin.

On this platform, we utilized an air-liquid interface (ALI) culture system to promote keratinocyte

differentiation in the cutaneous barrier[37]. The day following the filling of all gel layers, NHEKs were seeded in channel #1 and cultured for 2 days to proliferate sufficiently to form a thick layer. On the second day, HDLECs were seeded in channel #5, and the device was tilted at 45° to adopt the ALI culture conditions. Three days later, HDLECs on 2 mg/ml COL1 formed a confluent monolayer, whereas NHEKs developed a stable cutaneous barrier (Fig. 6a). The cutaneous barrier expressed keratin 14 (K14; a skin basal layer marker[38]), keratin 10 and loricrin (K10 and Lor; biomarkers of differentiated keratinocytes[39,40]) on Day 5 (upper panels in Fig. 6b). The HDLEC monolayer successfully expressed PROX1 and LYVE1 in three days (lower panels in Fig. 6b).

The cutaneous barrier prevents external environmental substances from invading the body[12,37]. Several fluorescence molecules, including 0.4 kDa fluorescein sodium salt and 4,40 kDa fluorescein isothiocyanate-dextran (FITC-dextran), were used to confirm the defensive capability. The molecules were applied to the formed cutaneous barrier, and the permeability was calculated from the fluorescence intensity graph. The acquired permeabilities for molecules ranging in size from 0.4 kDa to 40 kDa were comparable (Fig. 6c, d, S4a), whereas fluorescence molecules diffused rapidly across the non-confluent (leaky) cutaneous barrier (Fig. S4b, c). The permeability of a healthy cutaneous barrier was independent of molecular size and diffusion time (30, 60, 120 min) (Fig. S4c). This model resembles previous in vitro skin models, preventing the invasion of external substances with a size of 0.5 kDa[41]. With the cutaneous barrier and HDLEC single layer that reconstitutes the existing precollecting lymphatic vessel under the epidermis-like layer, we developed a microfluidic model of the human cutaneous lymphatic system.

Evaluation of lymphanax with a reconstituted cutaneous lymphatic system

The cutaneous lymphatic system was used to confirm the pro-lymphangiogenic effect of Lymphanax. Lymphanax was applied to the fully differentiated functional cutaneous barrier for six days (Fig. 6a). More lymphangiogenesis was observed in the V100 + L250 (applied to the cutaneous layer) group than in the V100 group (applied to the cutaneous layer) (Fig. 7a, S5a). We measured the vessel length, vessel number and vessel area and found that the number, area and length of neolymphatic vessels were increased under the Lymphanax-treated condition, similar to previous results without a cutaneous layer (Fig. S5b). As confirmed, the number of separated tip cells decreased (Fig. S5c). Additional quantification with the algorithm revealed that the average number, area and perimeter of total neolymphatic branches increased after treatment with 250 μg/ml Lymphanax (Fig. 7b). The number of nodes and the branch width differentiation were also greater in the V100 + L250 condition, whereas the average branch length was comparable across all conditions (Fig. 7b). Then, we confirmed the character of the neolymphatic vessels with the cutaneous barrier. As anticipated, there were no differences in the curvature, branch area, node radius, straight length of branches, branch width, or number of branches connecting nodes across all conditions (Fig. 7c). In addition, stable expression of all markers was observed in each lymphatic vessel after treatment with Lymphanax in the cutaneous layer (Fig. 7d). Consistent with our previous data presented in Fig. 5b, the V100 + L250 group expressed these markers more strongly than the V100 group (Fig. 7d).

The permeability test with the cutaneous barrier demonstrated that it could block 0.4 kDa molecules, which are smaller than saponin, the major component of Lymphanax (1.2 kDa)[42,43]. Therefore, the lymphangiogenic effect may be caused not only by the direct effect of leaked Lymphanax on the lymphatic vessel but also by the substances secreted from keratinocytes. Using ELISAs, we assessed molecules secreted from Lymphanax-treated NHEKs and found that only the VEGF-C concentration increased (Fig. S6a). NHEKs treated with Lymphanax at concentrations greater than 20 μg/ml exhibited cytotoxicity (Fig. S6b). Secreted VEGF-C, which is known to promote lymphangiogenesis, could be a potential candidate, but verification requires additional investigation[22].

Discussion

The essential function of the cutaneous lymphatic system, which consists of lymphatic vessels in the hypodermis, is to maintain skin homeostasis. As one of the largest organs in the human body, the skin produces a high level of interstitial fluid, which is effectively removed by the dense cutaneous lymphatic system. If this process does not occur, the skin will become swollen and cracked, allowing antigens and molecules from the outside to enter the body. This phenomenon is responsible for a vicious cycle of severe inflammation. Therefore, a comprehensive understanding of the skin and lymphatic system is necessary. Nonetheless, the absence of a research model for the cutaneous lymphatic system remains a barrier. Although animal models are used to study the complexity of the cutaneous lymphatic system, they do not accurately represent human responses. In addition, current in vitro models cannot accurately reflect the communications between the skin and lymphatic system because it is difficult to replicate these two conditions.

In this paper, we describe a microfluidic platform that contains precollecting lymphatic vessels beneath the functional cutaneous barrier and has the potential to evaluate lymphangiogenesis in the human cutaneous lymphatic system. First, we optimized three different collagen concentrations for stable formation of the

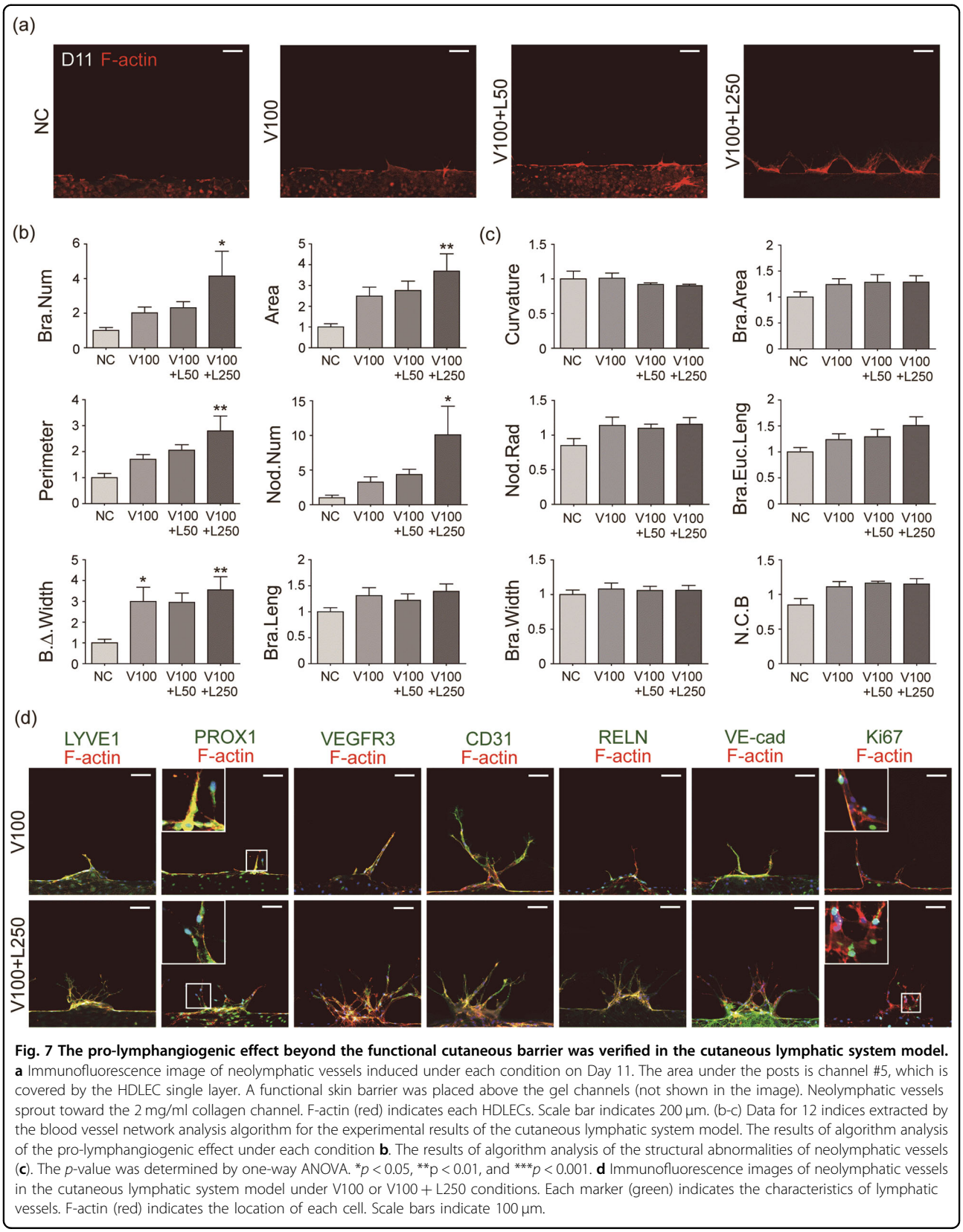

Fig. 7 The pro-lymphangiogenic effect beyond the functional cutaneous barrier was verified in the cutaneous lymphatic system model. **a** Immunofluorescence image of neolymphatic vessels induced under each condition on Day 11. The area under the posts is channel #5, which is covered by the HDLEC single layer. A functional skin barrier was placed above the gel channels (not shown in the image). Neolymphatic vessels sprout toward the 2 mg/ml collagen channel. F-actin (red) indicates each HDLECs. Scale bar indicates 200 μm. (b-c) Data for 12 indices extracted by the blood vessel network analysis algorithm for the experimental results of the cutaneous lymphatic system model. The results of algorithm analysis of the pro-lymphangiogenic effect under each condition **b**. The results of algorithm analysis of the structural abnormalities of neolymphatic vessels (**c**). The *p*-value was determined by one-way ANOVA. *$p < 0.05$, **$p < 0.01$, and ***$p < 0.001$. **d** Immunofluorescence images of neolymphatic vessels in the cutaneous lymphatic system model under V100 or V100 + L250 conditions. Each marker (green) indicates the characteristics of lymphatic vessels. F-actin (red) indicates the location of each cell. Scale bars indicate 100 μm.

cutaneous layer and lymphatic monolayer. COL1, with a high concentration in the middle layer, acted as a barrier to prevent direct contact and uncontrollable interruption between NHEKs and lymphatic vessels. Each cell preferred a particular concentration of COL1, and the three-channel design allowed the cocultured cutaneous components to remain healthy and functional. COL1 (3 mg/ml) was sufficient for NHEK cells to maintain confluence but insufficient for long-term experiments. COL1 (2 mg/ml) allowed lymphatic cells to form a confluent monolayer and engage in active spouting. ALI culture acquired via chip tilting induced keratinocyte differentiation into small substances blocking the cutaneous barrier (400 Da). Despite the successful development of a functional cutaneous barrier, the irregular direction of skin stratification posed a limitation (Fig. 6b). This limitation may be attributable to the insufficient duration of culture under an air-liquid interface (ALI) for the cells to become fully differentiated, as well as the increased chance for keratinocytes to interact with the surface of microfluidic channels. The cutaneous barrier used in this paper has a sufficient barrier function to prevent the penetration of small substances, but it is not completely differentiated and has imperfect inner layer alignment.

Lymphanax, which is an extract of specially fermented fresh ginseng and contains saponin family components, was evaluated for its lymphangiogenic effect. Intriguingly, basic 3D vessel-unit structures with similar node sizes and connected branches were maintained despite the vigorous lymphatic vessel growth observed under the influence of Lymphanax. The pro-lymphangiogenic effect of Lymphanax when applied to the cutaneous layer can demonstrate the molecule's potential for use in cosmetics. Lymphanax has a cytotoxic effect when applied directly to cultured NHEK cells at concentrations greater than 20 μg/ml. Even at much higher concentrations, we were unable to detect the cytotoxic effect of Lymphanax applied to the ALI-cultured cutaneous layer formed with NHEK cells in the microfluidic channel. We hypothesized that Lymphanax applied to the cutaneous layer leaked and induced a pro-lymphangiogenic effect, but we also discovered a weak indication that stimulating keratinocytes to secrete VEGF-C. Lymphanax has been identified as a stimulant that affects the lymphatic system beneath the cutaneous barrier, although the precise mechanism of Lymphanax in keratinocytes remains to be clarified through additional research.

We also demonstrated that the previously reported algorithm for vascular network analysis can be used to quantify 3D lymphangiogenesis. In 3D lymphatic vessels, the correlation between manually measured and automatically quantified data with the deep learning-based algorithm was confirmed. The algorithm also enabled us to monitor physiological 3D alterations in neolymphatic vessels. The potential effect of Lymphanax on a pro-lymphangiogenic effect could be easily verified with an additional effect on the stability of the lymphatic network structure. The algorithm improved the speed, objectivity, and precision of our platform, making them viable candidates for high-throughput lymphangiogenesis analysis platforms and models of the cutaneous lymphatic system. Investigations of the cutaneous lymphatic system can be conducted in a cost-effective and precise manner with the aid of this tool.

Protection, thermoregulation and sensation are three primary functions of skin[44]. The integration of sensory neurons is associated with thermoregulation and sensation[44]. The primary objective of this paper is to reconstitute the lymphatic system and confirm the regulatory ability of a molecule (Lymphanax) on the reconstituted lymphatic system. A skin barrier was added to corroborate that the capability is still present when the lymphatic system is located beneath the skin barrier. The inclusion of other cells, such as neurons, is expected to reproduce additional thermoregulatory and sensory skin functions in further research. The lymphatic system added to the skin layer may have potential applications, such as biosensors and infection research[45,46], through further development. This device serves as an alternative to animal models and has the potential to produce better results by utilizing human-derived cells, in light of the global trend toward animal experimentation prohibition. We therefore anticipate that these platforms will serve as valuable development tools for the pharmaceutical and cosmetics industries.

Acknowledgements
This work was supported by the National Research Foundation (NRF) grant funded by the Korea government (MSIT) (2022M3A9B6018217) and the Technology Innovation Program (No.20008413) funded by the Korea government (MSIT).

Author details
[1]KU-KIST Graduate School of Converging Science and Technology, Korea University, Seoul 02841, Republic of Korea. [2]School of Mechanical Engineering, Korea University, Seoul 02841, Republic of Korea. [3]Next&Bio Inc, Seoul 02841, Republic of Korea. [4]Basic Research & Innovation Division, AMOREPACIFIC R&I Center, Gyeonggi-do 17074, Republic of Korea. [5]Skincare Research Division, AMOREPACIFIC R&I Center, Gyeonggi-do 17074, Republic of Korea. [6]Center for Brain Technology, Brain Science Institute, Korea Institute of Science and Technology (KIST), Seoul 02792, Republic of Korea

Author contributions
M-S.K., S-E.C., M.K., P.J.P. and S.C. conceived the study and explained the experimental results. H-S.K., M-J.K., and S-W.C. developed the Lymphanax. M-S.K., S-E.C., J-C.A., S-J.O., P.J.P. and S.C. developed the microfluidic platform. D.H.C., E-J.S. and S.C. developed the vascular vessel network analysis algorithm and analyzed lymphangiogenesis by the algorithm. M-S.K., S-E.C., J-C.A. and D.L. performed the experiment and analyzed the data. M-S.K., S-E.C., M.K., P.J.P. and S.C. wrote the paper and Supplementary Information. All authors were involved in the discussion of the results and approved the final version of the manuscript.

Conflict of interest
The authors declare no competing interests.

Supplementary information The online version contains supplementary material available at https://doi.org/10.1038/s41427-023-00527-3.

Received: 12 April 2023 Revised: 11 November 2023 Accepted: 21 November 2023
Published online: 02 February 2024

References

1. Margaris, K. N. & Black, R. A. Modelling the lymphatic system: Challenges and opportunities. *J. R. Soc. Interface* **9**, 601–612 (2012).
2. Null, M. & Agarwal, M. *Anatomy, Lymphatic System*. (StatPearls Publishing: Treasure Island (FL), 2018. http://europepmc.org/abstract/MED/30020619 at.
3. Lund, A. W., Medler, T. R., Leachman, S. A. & Coussens, L. M. Lymphatic vessels, inflammation, and immunity in skin cancer. *Cancer Discov.* **6**, 22–35 (2016).
4. Eyerich, S., Eyerich, K., Traidl-Hoffmann, C. & Biedermann, T. Cutaneous Barriers and Skin Immunity: Differentiating A Connected Network. *Trends Immunol.* **39**, 315–327 (2018).
5. Stacker, S. A., et al. Lymphangiogenesis and lymphatic vessel remodelling in cancer. *Nat. Rev. Cancer* **14**, 159–172 (2014).
6. Jeltsch, M. et al. *Hyperplasia of Lymphatic Vessels in VEGF-C Transgenic Mice*. https://doi.org/10.1126/science.276.5317.1423 (1997).
7. Deng, Y., Zhang, X. & Simons, M. Molecular controls of lymphatic VEGFR3 signaling. *Arterioscler Thromb. Vasc. Biol.* **35**, 421–429 (2015).
8. Henderson, A. R., Choi, H. & Lee, E. Blood and lymphatic vasculatures on-chip platforms and their applications for organ-specific in vitro modeling. *Micromachines* **11,** 147 (2020).
9. Olszewski, W. L. The Lymphatic System in Body Homeostasis: Physiological Conditions. *Lymphat. Res. Biol.* **1**, 11–24 (2003).
10. Alitalo, K., Tammela, T. & Petrova, T. V. Lymphangiogenesis in development and human disease. *Nature* **438**, 946–953 (2005).
11. Christiansen, A. & Detmar, M. Lymphangiogenesis and Cancer. *Genes Cancer* **2**, 1146–1158 (2011).
12. Kolarsick, P. A. J., Kolarsick, M. A. & Goodwin, C. Anatomy and Physiology of the Skin. *J. Dermatol. Nurses Assoc.* **3**, 203–213 (2011).
13. Petrova, T. V. & Koh, G. Y. Organ-specific lymphatic vasculature: From development to pathophysiology. *Journal of Experimental Medicine* **215**, 35–49 (2018).
14. Stanley, G. & Rockson, M. D. Lymphedema. *Am. J. Med.* **110**, 288–298 (2001).
15. Bruyère, F. & Noël, A. Lymphangiogenesis: in vitro and in vivo models. *FASEB J.* **24**, 8–21 (2010).
16. Bruyère, F. et al. Modeling lymphangiogenesis in a three-dimensional culture system. *Nat. Methods* **5**, 431–437 (2008).
17. Halldorsson, S., Lucumi, E., Gómez-Sjöberg, R. & Fleming, R. M. T. Advantages and challenges of microfluidic cell culture in polydimethylsiloxane devices. *Biosens. Bioelectron.* **63**, 218–231 (2015).
18. Cui, P. & Wang, S. Application of microfluidic chip technology in pharmaceutical analysis: A review. *J. Pharm. Anal.* **9**, 238–247 (2019).
19. Kim, S., Chung, M. & Jeon, N. L. Three-dimensional biomimetic model to reconstitute sprouting lymphangiogenesis in vitro. *Biomaterials* **78**, 115–128 (2016).
20. Cho, Y. et al. Three-Dimensional In Vitro Lymphangiogenesis Model in Tumor Microenvironment. *Front. Bioeng. Biotechnol.* **9**, 697657 (2021).
21. Li, J. et al. Total saponins of panaxnotoginseng promotes lymphangiogenesis by activation VEGF-C expression of lymphatic endothelial cells. *J. Ethnopharmacol.* **193**, 293–302 (2016).
22. Yu, J., Mao, L., Guan, L., Zhang, Y. & Zhao, J. Ginsenoside Rg1 enhances lymphatic transport of intrapulmonary silica via VEGF-C/VEGFR-3 signaling in silicotic rats. *Biochem Biophys. Res Commun.* **472**, 182–188 (2016).
23. Miranda, I. et al. Properties and applications of PDMS for biomedical engineering: A review. *J. Funct. Biomater.* **13,** 2 (2022).
24. Shumbula, N. P. et al. Evaluating the antimicrobial activity and cytotoxicity of polydopamine capped silver and silver/polydopamine core-shell nanocomposites. *Arab. J. Chem.* **15**, 103798 (2022).
25. Jain, R. K. Molecular regulation of vessel maturation. *Nat. Med.* **9**, 685–693 (2003).
26. Herbert, S. P. & Stainier, D. Y. R. Molecular control of endothelial cell behaviour during blood vessel morphogenesis. *Nat. Rev. Mol. Cell Biol.* **12**, 551–564 (2011).
27. Choi, D.-H. et al. Analyzing angiogenesis on a chip using deep learning-based image processing. *Lab Chip*. https://doi.org/10.1039/D2LC00983H (2023).
28. moonchildz. angio_analysis. (2023). at https://github.com/moonchildz/angio_analysis.
29. Shin, Y. et al. In vitro 3D collective sprouting angiogenesis under orchestrated ANG-1 and VEGF gradients. *Lab Chip* **11**, 2175–2181 (2011).
30. Jackson, D. G., Prevo, R., Clasper, S. & Banerji, S. LYVE-1, the lymphatic system and tumor lymphangiogenesis. *Trends Immunol.* **22**, 317–321 (2001).
31. Wilting, J. et al. The transcription factor Prox1 is a marker for lymphatic endothelial cells in normal and diseased human tissues. *FASEB J.: Off. Publ. Federation Am. Societies Exp. Biol.* **16**, 1271–1273 (2002).
32. Kaipatnen, A. et al. Expression of the fms-like tyrosine kinase 4 gene becomes restricted to lymphatic endothelium during development. *Med. Sci.* **92**, 3566–3570 (1995).
33. van Mourik, J. A., Leeksma, O. C., Reinders, J. H., de Groot, P. G. & Zandbergen-Spaargaren, J. Vascular endothelial cells synthesize a plasma membrane protein indistinguishable from the platelet membrane glycoprotein IIa. *J. Biol. Chem.* **260**, 11300–11306 (1985).
34. Ji, R.-C., Kato, S., Shimoda, H. & Miura, M. Lymphatic endothelial cells, lymphangiogenesis, and extracellular matrix. *Res. Biol.* **4**, 83–100 (2006).
35. Yao, L. C., Baluk, P., Srinivasan, R. S., Oliver, G. & McDonald, D. M. Plasticity of button-like junctions in the endothelium of airway lymphatics in development and inflammation. *Am. J. Pathol.* **180**, 2561–2575 (2012).
36. Gerdes, J. et al. Cell cycle analysis of a cell proliferation-associated human nuclear antigen defined by the monoclonal antibody Ki-67'. *J. Immunol.* **133**, 1710–1715 (1984).
37. Zuniga, K. et al. Keratin Promotes Differentiation of Keratinocytes Seeded on Collagen/Keratin Hydrogels. *Bioengineering* **9**, 559 (2022).
38. Alam, H., Sehgal, L., Kundu, S. T., Dalal, S. N. & Vaidya, M. M. Novel function of keratins 5 and 14 in proliferation and differentiation of stratified epithelial cells. *Mol. Biol. Cell* **22**, 4068–4078 (2011).
39. Moll, R., Divo, M. & Langbein, L. The human keratins: Biology and pathology. *Histochem. Cell Biol.* **129**, 705–733 (2008).
40. Nithya, S., Radhika, T. & Jeddy, N. Loricrin - An overview. *J. Oral Maxillofac. Pathol.* **19**, 64–68 (2015).
41. Bos, J. D. & Meinardi, M. M. H. M. The 500 Dalton rule for the skin penetration of chemical compounds and drugs. *Exp. Dermatol.* **9**, 165–169 (2000).
42. Li, L. et al. Detection of saponins in extract of Panax notoginseng by liquid chromatography-electrospray ionisation-mass spectrometry. *Anal. Chim. Acta* **536**, 21–28 (2005).
43. National Center for Biotechnology Information (2023). PubChem Compound Summary for CID 198016, Saponin. Retrieved March 3, 2023 from https://pubchem.ncbi.nlm.nih.gov/compound/Saponin.
44. Ahn, J. et al. Modeling of three-dimensional innervated epidermal like-layer in a microfluidic chip-based coculture system. *Nat. Commun* **14**, 1488 (2023).
45. Xu, Y. et al. Construction of a 980 nm laser-activated Pt(II) metallacycle nanosystem for efficient and safe photo-induced bacteria sterilization. *Sci. China Chem.* **66**, 155–163 (2023).
46. Xu, Y. et al. Long wavelength-emissive Ru(II) metallacycle-based photosensitizer assisting in vivo bacterial diagnosis and antibacterial treatment. https://doi.org/10.1073/pnas (2022).